JOURNAL OF MATERIALS SCIENCE 39 (2004) 1773–1778

Combustion synthesis, sintering and magnetical properties of nanocristalline Ni-Zn ferrites doped with samarium

ANA CRISTINA F. M. COSTA
Federal University of Paraíba, Department of Materials Engineering, 58970-000 Campina Grande PB, Brazil

MÁRCIO R. MORELLI, RUTH H. G. A. KIMINAMI
Federal University of São Carlos, Department of Materials Engineering, 13565-905 São Carlos SP, Brazil
E-mail: ruth@power.ufscar.br

An investigation was made of combustion synthesis to uniformly incorporate small amounts of samarium additive into nanocrystalline $Ni_{0.5}Zn_{0.5}Fe_{2-x}Sm_xO_4$ ($0.0 \leq x \leq 0.1$) nanopowders (≈26–20 nm particle size). The effect of the addition of the rare-earth ion samarium on the microstructure, relative density and magnetic properties of the Ni-Zn ferrite obtained by combustion reaction was studied. The samples were uniaxially compacted by dry pressing, sintered at 1200°C/2 h, and characterized by bulk and apparent density, XRD, SEM and magnetic properties. The nanopowder samples without additive displayed an average grain size of 2.87 μm, while the addition of 0.05; 0.075 and 0.1 wt% Sm was found to inhibit grain growth, decreasing the average grain size to 0.77; 0.68 and 0.62 μm, respectively. The relative density was found to increase with the addition of samarium (>98.00% of the theoretical density). The samples without additive showed higher hysteresis parameter values. © *2004 Kluwer Academic Publishers*

1. Introduction

Ni-Zn ferrites have been studied extensively in both scientific and technological contexts, primarily due to their applicability in many electronic devices, with high permeability at high frequency, remarkably high electrical resistivity and reasonable cost [1, 2].

Ni-Zn ferrites have a basic AB_2O_4 with an inverse-spinel structure and the Fd3m space group. The chemical formula can be written as $(Zn_xFe_{1-x})[Ni_{1-x}Fe_{1+x}]O_4$. The crystal structure involves two crystallographically distinct sites called tetrahedral *A* sites and octahedral *B* sites, where Ni^{2+} ions prefer *B* sites and Zn^{2+} ions prefer *A* sites. The metal-ions (Fe^{3+}) in the spinel lattice involve tetrahedral *A* and octahedral *B* sites [3]. It is a prototypical ferromagnetic material belonging to a group of soft ferrite materials, whose chemical composition consists of a solid solution of NiO, ZnO and Fe_2O_3 oxides. Iron oxide in the hematite form (α-Fe_2O_3) constitutes around 70% of the composition's weight [4].

Ni-Zn ferrites are advantageous over other soft magnetic materials for use at high frequencies because they possess high electrical resistivities combined with useful ferrimagnetic properties. The properties of ferrites are highly sensitive to the preparation methodology, sintering conditions and impurity levels present in or added to them [5–14]. The essence of these studies reveals that, although it is difficult to prepare a ferrite with only good properties, a satisfactory result can be achieved by improving the most required property at the cost of the least required one for a particular application [11].

The electrical and magnetic properties desired specifically in these materials depend, to a large extent, on the original characteristics of the powders used (their forms, average size and particle size distribution, degree of agglomeration, etc.), which affect the densification and microstructure of the final product. On the other hand, these properties depend heavily on the oxidation state and cation distributions at the octahedral *B* site and tetrahedral *A* site lattice [2].

Ni-Zn ferrites are widely used as transformers in switch-mode power supply (SMPS). The main reason for using ferrites in transformer cores is that their loss of eddy currents is very low. A ferrite material that is to be used in a SMPS should have a high saturation magnetization, high amplitude permeability, and low power losses [15]. To improve the electrical and magnetic properties of Ni-Zn ferrite, the ferrite must have a dense, homogeneous, fine-grained microstructure. Additionally, small amounts of cationic substitutions are usually used. Three types of additives are normally used for incorporation into the basic ferrite. The first type, e.g., V_2O_5 [5] and Bi_2O_3 [7], acts indirectly via liquid phase formation, influencing the microstructure's development during sintering. Addition of the second type

modifies the grain boundary chemistry and increases the grain boundary resistivity, e.g., SiO_2, CaO [8, 10] and Ta_2O_5 [10]. The third type of cation is soluble in the spinel lattice, such as TiO_2, SnO_2 [9, 10], etc. These additives affect the intrinsic properties of magnetization, anisotropy and electrical resistivity.

Among the several additives studied in the literature, samarium, specifically, has resulted in quite significant values of the magnetic properties of the Cu-Zn ferrite [15]. According to Sattar *et al.* [15], their Sm-doped sample ($Cu_{0.5}Zn_{0.5}Fe_{2-x}Sm_xO_4$) gave an especially promising result from the technological point of view, with an increase of ≈60% in relative permeability compared to the unsubstituted sample. Both the lattice parameters and the Curie temperatures were found to be nearly constant.

Based on the satisfactory results obtained with Cu-Zn ferrite, this work describes the influence of the addition of the rare-earth ion samarium on the microstructure, relative density and magnetic properties of the Ni-Zn ferrite nanopowder obtained by combustion reaction.

2. Experimental methods

Fine particle oxides of Ni-Zn-Sm ferrite with nominal composition of $Ni_{0.5}Zn_{0.5}Fe_{2-x}Sm_xO_4$, with $x = 0.0$; 0.05; 0.075 and 0.1% mol, were prepared for combustion reaction using urea as fuel. Details of the experimental procedure are given in our previous work [16–21]. The compositions were dubbed C05, C05I, C05II and C05III, respectively. The materials used were iron nitrate—$Fe(NO_3)_3{\cdot}9H_2O$ (Merck), zinc nitrate—$Zn(NO_3)_2{\cdot}6H_2O$ (Merck), nickel nitrate—$Ni(NO_3)_2{\cdot}6H_2O$ (Merck), samarium nitrate—$Sm(NO_3)_3{\cdot}9H_2O$ and urea—$CO(NH_2)_2$ (Synth). Stoichiometric compositions of metal nitrate and urea were calculated using the total oxidizing and reducing valencies of the components, which serve as the numerical coefficients for the stoichiometric balance, so that the equivalence ratio Φ_c is unity and the energy released is maximum [18]. Ferrite nanoparticles without and with additive prepared by the present method can easily form well-crystallized particles with a large surface area in the range of 43–57 m^2/g. The resulting powders showed extensive XRD line broadening and the crystallite sizes calculated from the XRD line broadening were in the nanometer range (26–20 nm).

Ni-Zn compacted samples sintered at 1200°C/2 h were characterized by X-ray diffraction (Kristaloflex D5000, Cu K_α with a Ni filter, and scanning rate of 2°2θ/min, in a 2θ range of 20–60°). The bulk and apparent density were calculated by dimension and weight measurements, using the Archimedean principle. *B-H* loop measurements were performed on toroids with primary and secondary windings of 26 SWG enameled copper wire, using a hysteresis loop tracer (TCH 8600-B). All the measurements were taken at room temperature. The maximum permeability (μ_{max}) was determined for the tangent of the hysteresis *B-H* loop, Fig. 1, where the displacements of the irreversible domain wall occur [22]. Fig. 2 shows the toroids sintered and wound with 26 SWG enameled copper wire. The as-prepared

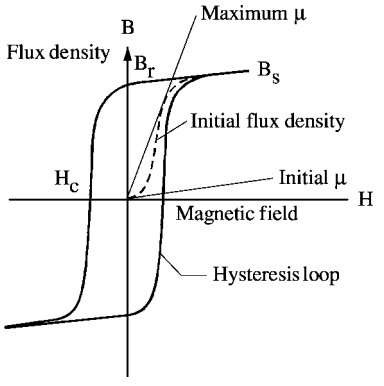

Figure 1 Loop *B-H* of the magnetization and desmagnetization.

Figure 2 Representation of the toroids sinterized to 1200°C/2 h and after windings of 26 SWG enameled copper wire.

combustion reaction powders and the microstructure of the polished surfaces of the sintered samples were analyzed by scanning electron microscopy (Philips XL30 FEG)—SEM.

3. Results

3.1. Ray-X diffraction

To identify the possible formation of second phase with the addition of the Sm^{3+} concentration in the $Ni_{0.5}Zn_{0.5}Fe_2O_4$ (C05) system, an X-ray diffraction analysis was made of the samples with 0.1% mol of Sm^{3+} (C05III). Fig. 3 presents the X-ray diffractogram

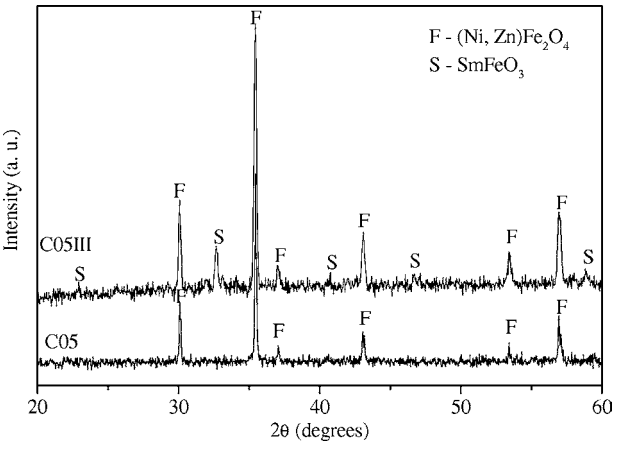

Figure 3 X-ray diffratogram of the samples of the systems C05 ($Ni_{0.5}Zn_{0.5}Fe_2O_4$) and C05III ($Ni_{0.5}Zn_{0.5}Fe_{1.90}Sm_{0.1}O4$) sintering at 1200°C/2 h.

of systems C05 and C05III obtained by combustion reaction and sintered at 1200°C/2 h. As can be seen, the C05 system (without additive) presented only a Ni-Zn ferrite cubic phase, while the C05III system (0.1% of Sm^{3+}) also presented an ortorhombic second phase of iron samarium oxide ($SmFeO_3$).

3.2. Microstructure

The microstructures were characterized by SEM (scanning electronic microscopy) on the polished surfaces of the samples sintered at 1200°C/2 h with a heating rate of 5°C/min, as shown in Fig. 4. System C05 (without additive), Fig. 4a showed a monophasic and homogeneous microstructure with an average grain size of 2.87 ± 1.11 μm. System C05I (with 0.05% Sm^{3+} mol), Fig. 4b, displayed a bi-phasic microstructure constituted of a matrix of dark grains and a second phase formed of clear grains located among the grains of the matrix. The average grain size determined was 0.27 ± 0.08 μm for the clear grains and 0.77 ± 0.29 μm for the dark matrix grains. A comparison of the average size of the dark grains of this system with those of the C05 system (without additive) clearly revealed that the addition of 0.05% mol of samarium inhibited the grain growth by about 73%.

Fig. 4c and d show the micrographs of the C05II (with 0.075% Sm^{3+} mol) and C05III (with 0.1% Sm^{3+} mol) systems. As can be seen, the same behavior as that observed in the C05I system prevailed in both cases, i.e., a microstructure composed of two different phases. The first phase consisted of a matrix of dark grains and the second phase was made up of a samarium-rich precipitate at the junctions of the matrix's grains. It was clearly observed that the increase in samarium concentration increased the amount of precipitate, thereby reducing the average grain size of the matrix and increasing the average grain size of the precipitate. The average sizes of matrix and precipitate grains were, respectively 0.68 and 0.28 μm for the C05II system and 0.30 and 0.62 μm for the C05III system. Comparing the average size of the dark grains (matrix) of these systems with the average grain size of the C05 system (without additive, 2.87 μm), it was found that the addition of 0.075 and 0.1% in mol of the additive inhibited grain growth by approximately 76 and 78%, respectively.

3.3. Density

Results of the measurements of apparent porosity, geometric density Dg, apparent density and the respective relative densities for the systems without and with additive (C05, C05I, C05II and C05III), after sintering at 1200°C/2 h showed, an increase in the samarium (Sm^{3+}) concentration tended to increase the samples'

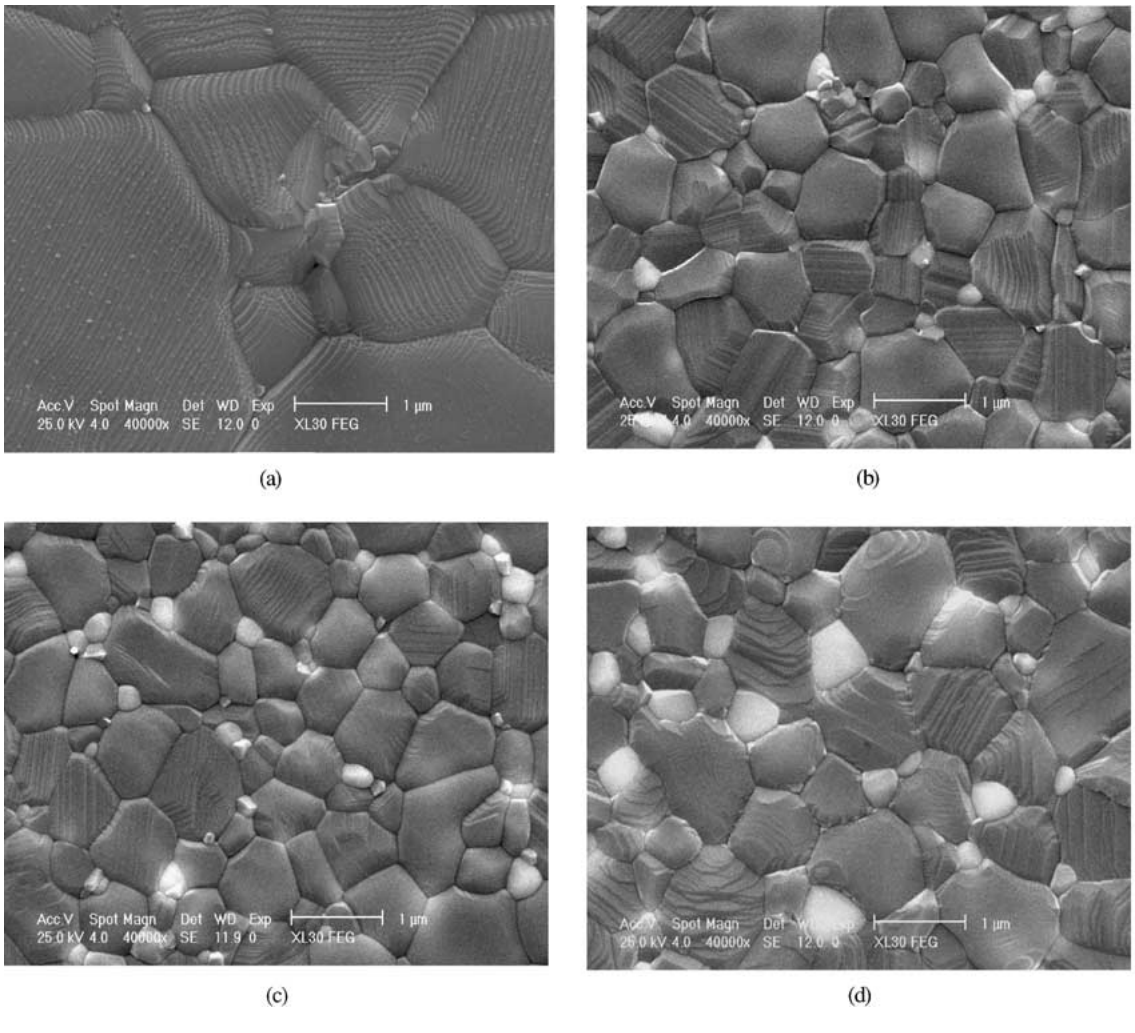

Figure 4 Microstructure obtained by SEM after sintering at 1200°C/2 h and heating rate at 5.0°C/min: (a) C05, (b) C05I, (c) C05II e and (d) C05III.

density (increased densification) and, hence, to reduce their porosity. The apparent density values were slightly higher than the geometric density values for the samples doped with 0.05 and 0.075% mol of samarium. In the case of the samples of the system without and with 0.1% of samarium, these two parameters were of the same order of magnitude.

The $Ni_{0.5}Zn_{0.5}Fe_2O_4$ nanopowder without additive displayed a relative density of about 95% of the theoretical density, while the chemical addition of 0.05; 0.075 and 0.1 wt% Sm^{3+} to the nanopowder caused the relative density to increase. This clearly indicates that increasing the Sm^{3+} concentration increased the relative density of the samples, which reached values of around 100% of the theoretical density. These values are higher than those reported by Sattar *et al*. [15] for Ni-Cu ferrite doped with samarium (92.4% TD) obtained by oxide mixture and sintered at 1000°C/6 h. In agreement with Sattar *et al*. [15], the samples with samarium presented the smallest relative value when compared with the unsubstituted samples. This phenomenon was attributed to the formation of SmO_2 during the sintering process. SmO_2 favors the growth of grains with large inner pores. A different behavior was observed when the addition of Sm^{3+} was used as a substitute in the Ni-Zn ferrite of this study. The formation of the second $SmFeO_3$ phase was found to favor the inhibition of grain growth and to increase the relative density in comparison to the unsubstituted samples.

3.4. Magnetical properties

The dependence of the maximum flux density (B) on the applied magnetic field (H) by loop hysteresis B-H of the C05, C05I, C05II and C05III systems samples sintered at 1200°C/2 h is shown in Table I and the results of hysteresis measurements (coercive field H_c, remanent flux density B_r, maximum flux density B_{max}, loss hysteresis P_H and maximum permeability μ_{max}) and the average grain sizes of the C05, C05I, C05II and C05III systems sintered at 1200°C/2 h are presented and an increase in H_c is observed as the concentration of samarium increases. This increase is attributed to a decrease in grain size.

The results depicted in Fig. 4b, c and d evidence that the addition of samarium to the $Ni_{0.5}Zn_{0.5}Fe_2O_4$ system inhibits grain growth owing to the formation of a second phase ($SmFeO_3$ precipitate) between the ferrite grains. Thus, because the magnetic properties (magnetization, permeability) are dependent on the domains' wall movement, large grains tend to consist of a greater number of domain walls. The magnetization/demagnetization caused by domain wall movement requires lower energy compared to that required for domain rotation. Therefore, the larger the grain size, the easier the displacement. Hence, it was to be expected that the increase in the concentration of Sm^{3+} in the $Ni_{0.5}Zn_{0.5}Fe_2O_4$ systems did not cause an increase in the hysteresis parameters, considering the decrease of the Fe-Fe interactions due to the reduction of the Fe^{3+} concentration in B sites caused by the substitution of the Sm^{3+} ion. However, to control the eddy current, which is an important property when operating at high frequencies (above 500 MHz), the addition of samarium can be effective.

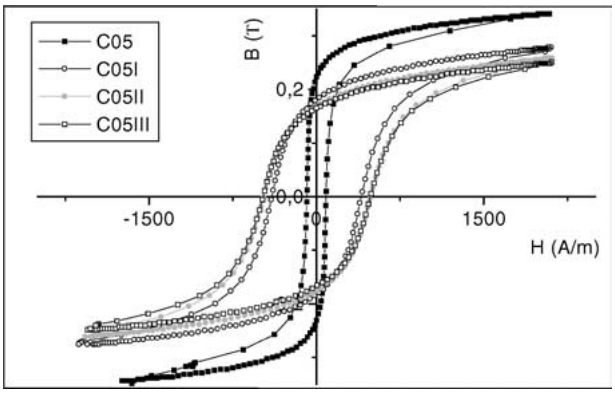

Figure 5 Loops hysteresis (magnetization) for samples of the system $Ni_{0.5}Zn_{0.5}Fe_{2-x}O_4$ with $x = 0.0$; 0.05; 0.075 e 0.1% mol samarium sinterized at 1200°C/2 h and heating rate at 5°C/min; $f = 1$ kHz; $e = 4.0$ mm e $H = 2000$ A/m.

The area of the B-H loops in Fig. 5 reveals the characteristic soft or permeable magnetic material of the C05 and C05I systems. The C05II and C05III systems can be classified as intermediate magnetic for magnetic recording. A slight reduction can be observed in the coercive field, as well as an increase of the maximum flux density and permeability in the C05I (0.05% de Sm^{3+}) system compared with the doped C05II (0.075% de Sm^{3+}) and C05III (0.1% de Sm^{3+}) systems.

Table II shows the direct dependence of the hysteresis parameter on the grain size. In this case, the effect of the microstructure on the magnetic properties for operation at low frequencies, which was the case of this study, was stronger than the effect of the composition (dependent on each system's intrinsic characteristics). The higher Sm^{3+} concentration increased the coercive field and the hysteretic losses, reducing the samples' magnetization and permeability. Therefore, the C05 system (without additive) presented the best results in terms of hysteresis parameters for use as soft magnetic devices at low frequencies. The C05I system resulted in magnetic parameters that were within the range of theoretical values for Ni-Zn ferrite, i.e., 0.30–0.40 T for

TABLE I Characteristics physics of the samples of the system $Ni_{0.5}Zn_{0.5}Fe_{2-x}Sm_xO_4$ without and with additive of 0.05; 0.075 and 0.1% mol samarium obtained by combustion reaction

Systems	D_g (g/cm^3)	D_{vol}/D_t (%)	D_a (g/cm^3)	D_a/D_t (%)	Pa (%)
C05	5.02 ± 0.06	95.40 ± 1.00	5.01 ± 0.05	95.40 ± 0.93	1.51 ± 0.48
C05I	5.22 ± 0.03	99.40 ± 0.61	5.25 ± 0.02	99.80 ± 0.45	0.99 ± 0.46
C05II	5.19 ± 0.05	98.70 ± 0.98	5.26 ± 0.01	100.00 ± 0.25	0.0
C05III	5.26 ± 0.04	100.00 ± 0.80	5.26 ± 0.02	100.00 ± 0.29	0.0

TABLE II Physical characteristics and hysteresis parameters of the samples of the system $Ni_{0.5}Zn_{0.5}Fe_{2-x}O_4$ with $x = 0.0$; 0.05; 0.075 e 0.1% mol Sm^{3+} sinterized at 1200°C/2 h and heating rate at 5°C/min. $f = 1$ kHz; $e = 4.0$ mm and $H = 2000$ A/m

Systems	C05	C05I	C05II	C05III
Average grain size (μm)	2.87 ± 1.11	0.77 ± 0.29	0.68 ± 0.25	0.62 ± 0.26
	Hysteresis parameters ($f = 1$ kHz; $e = 4.0$ mm and $H = 2000$ A/m)			
H_c (A/m)	92.73 ± 3.40	294.31 ± 5.33	397.45 ± 9.64	480.06 ± 9.53
$B_{máx}$ (T)	0.35 ± 0.01	0.33 ± 0.01	0.30 ± 0.01	0.28 ± 0.01
$\mu_{máx}$	776.54 ± 87.71	403.21 ± 49.81	334.48 ± 11.25	308.28 ± 10.95
P_H (W/kg)	41.67 ± 5.38	49.54 ± 3.19	69.21 ± 1.30	87.54 ± 5.40

flux density and 10–1000 for permeability [23]. The magnetization and permeability values obtained for the C05II and C05III systems render them applicable as intermediate magnetic devices for recording purposes. One feature observed was that the addition of Sm^{3+} greatly contributed toward achieving high relative density in Ni-Zn-Sm ferrites.

As shown in Table II, the system with 0.05% of Sm^{3+} (C05I) presented a main phase with average grain size 73% smaller than that of the system without additive (C05). However, the magnetization and permeability results for this system were, respectively, only 5.7 and 48.1% lower than those of the system without additive. The addition of Sm^{3+} to the $Ni_{0.5}Zn_{0.5}Fe_2O_4$ system probably impaired the magnetic properties when analyzed at a frequency of 1 KHz, due to the significant reduction in grain size with the increase of the Sm^{3+} concentration.

The predominant losses in Ni-Zn ferrite are hysteresis and eddy current at operating frequencies lower than the relaxation frequency of the wall displacement. The loss in hysteresis depends on the magnetostriction, magnetocrystalline anisotropy, saturation magnetization and microstructure. The eddy current loss depends on the eddy current circuit dimension and electric resistivity, which are microstructure dependent. The eddy current can be reduced by increasing the resistivity of the ferrite core, which depends on the grain boundary resistivity and the grain resistivity. A small grain size, which increases the resistivity by maximizing the grain boundary surface, increases the relaxation frequency as well; however, it decreases the permeability and increases the coercive field [10]. According to Drofenik *et al*. [24], at low operating frequencies, the eddy current is proportional to the average grain size and inversely proportional to the resistance of the grain boundary. On the other hand, at high frequencies, the loss of eddy current is determined by grain size, grain boundary thickness and permissivity. Thus, the reduction of grain size caused by the addition of samarium contributes beneficially to control eddy current losses by producing an overall increase of resistivity at the grain boundary.

4. Conclusions

In conclusion, the combustion synthesis is a versatile process to synthesize Ni-Zn ferrite on a nanophase-scale and the results presented here indicate that small amounts of samarium incorporated into Ni-Zn ferrite can influence the materials' properties. The XRD of the samarium-doped samples revealed that the major phase of the Ni-Zn ferrite was cubic spinel, with a small amount of samarium iron oxide ($SmFeO_3$) as secondary phase. The addition of samarium to the $Ni_{0.5}Zn_{0.5}Fe_2O_4$ system inhibited grain growth and increased the samples' final density, resulting in Ni-Zn-Sm ferrites with a relative density of 98 to 100% of the theoretical density. The 73, 76 and 78% reduction of the grain size of the samarium-doped samples compared with that of the samples without samarium impaired the magnetic properties, restricting the material to low frequency applications of 1 kHz. The values of maximum flux density, coercive field, maximum permeability and hysteresis loss of the systems with 0.05; 0.075 and 0.1% mol of samarium ranged from 0.33–0.28 T; 294.31–480.06 A/m; 403.21–308.28; and 45.62–87.54 W/kg, respectively.

Acknowledgement

The authors gratefully acknowledge the financial support of CAPES and CNPq (Brazil).

References

1. K. ISHINO and Y. NARUMIYA, *Ceram. Soc. Bull.* **66** (1987) 1469.
2. L. ZHIYUAN, X. MAOREN and Z. J. OINGQIU, *Magn. Magn. Mater.* **219** (2000) 9.
3. F. SAITO, T. TOYODA, T. MORI, M. TANAKA, K. HIRANO and S. SASAKI, *Phys.* B **270** (1999) 35.
4. K. S. RANE, V. M. S. VERENKAR and P. Y. J. SAWANT, *Mater. Sci. Mater. Electron.* **10** (1999) 133.
5. G. C. JAIN, *et al*., *IEEE Trans. Magn.* **18**(2) (1982) 776.
6. S. F. WANG, *et al*., *J. Magn. Magn. Mater.* **220** (2000) 129.
7. H. T. KIM and H. B. IM, *IEEE Trans. Magn.* **18**(6) (1982) 1541.
8. N. LIN, R. K. MISHRA and G. THOMAS, *ibid.* **18**(6) (1982) 1544.
9. U. KONIG, *Appl. Phys.* **4** (1974) 237.
10. A. ZNIDARSIC, M. LIMPEL and M. DROFENIK, *IEEE Trans. Magn.* **31**(2) (1995) 950.
11. B. PARVATHEESWARA RAO, P. S. V. SUBB RAO and K. H. RAO, *ibid.* **33**(6) (1997) 4454.
12. E. SILEO, R. ROTELO and S. JACOBO, *Physica* B **320**(1–4) (2002) 257.
13. E. REZLESCUE, N. REZLESCUE, P. POPA, L. REZLESCUE and C. PASNICU, *Phys. Stat. Sol.* (a) **162** (1997) 673.
14. N. REZLESCU, E. REZLESCU, C. PASNICU and M. L. CRAUS, *J. Phys. Condens. Matter* **6** (1994) 5707.
15. A. A. SATTAR, *et al*., *Phys. Stat. Sol.* **171** (1999) 563.
16. A. C. F. M. COSTA (in Portuguese) Thesis, Materials Engineering Dept., Federal University of São Carlos, Brazil, 2002.

17. A. C. F. M. COSTA, M. R. MORELLI and R. H. G. A. KIMINAMI, *J. Mater. Syn. Proc.* (2002) 86.
18. R. H. G. A. KIMINAMI and J. KONA, (19) (2001) 156.
19. A. C. F. M. COSTA, E. TORTELLA, M. J. KAUFMAN, M. R. MORELLI and R. H. G. A. KIMINAMI, *J. Mater. Sci.* **37** (2002) 1.
20. *Idem.*, *Mater. Sci. For.* **403** (2002) 57.
21. S. R. JAIN and K. C. ADIGA, *Combust. Flame* **40** (1981) 71.
22. R. W. CAHAN and P. HAASEN (ed.), "Phys. Metall" (Physics Publishing, North-Holland, 1983).
23. A. GOLDMAN, "Engineered Material Handbook" (ASM International, Metal Park, 1991) Vol. 4, p. 1161.
24. M. DROFENIK, A. ZNIDARSIC and I. ZAJC, *J. Appl. Phys.* **82**(1) (1997) 333.

Received 20 September 2002
and accepted 15 October 2003